Functional Polysaccharide Composite Nanoparticles from Cellulose Acetate and Potential Applications

Martin R. Kulterer, Victoria E. Reichel, Rupert Kargl, Stefan Köstler, Velina Sarbova, Thomas Heinze, Karin Stana-Kleinschek, and Volker Ribitsch**

An in situ technique for preparing composite nanoparticles from hydrophobic cellulose acetate and hydrophilic polysaccharides using nanoprecipitation is presented. This technique allows the nanoparticles' surface properties to be tuned very specifically. Spherical, narrow-size-distributed composite nanoparticles of different size, charge, functionality, and increased stability can be generated by using hydroxyethyl cellulose, carboxymethyl cellulose, low molecular weight chitosan, and amino cellulose. The influence of the pH and hydrophilic polysaccharide content in the particle formation is shown. The pH- and ionic strength- effective zeta-potential functions are evidence of the presence of functional polysaccharides at the nanoparticle surface. The in situ technique is compared with the adsorption of hydrophilic polysaccharides onto cellulose acetate nanoparticles in two steps. The great potential of in situ prepared composite nanoparticles in the pharmaceutical industry and bio- or food technology, as carriers of hydrophobic substances in aqueous media and for specific surface modifications, e.g., to selectively introduce strong antimicrobial properties, is illustrated.

1. Introduction

During the last decade, the design of polysaccharide based nanoparticles and nanocapsules has become an emerging field of research with various applications in the pharmaceutical industry, medicine, and bio and food technology.[1–4] The advantage of such nanoparticles is the fact that polysaccharides are inexpensive, stable, biodegradable, and biocompatible macromolecules, providing an enormous chemical and structural variability.

Even though many polysaccharides are able to form nanoparticles in aqueous media, their applicability is often limited by the polysaccharides hydrophilic character. This can make it more difficult to entrap hydrophobic substances such as drugs or dyes. In addition particles that are formed from one type of polysaccharide are limited regarding their applicability.

To overcome these problems, the aim has to be for polysaccharide nanoparticles composed of hydrophobic domains and variable surface functionalities. A suitable way of generating nanoparticles with hydrophobic and functional hydrophilic domains is the self-assembly of amphiphilic polysaccharide-based copolymers.[5] The main drawback of this method is the time consuming and chemical intensive synthesis of polysaccharide-based copolymers. As an alternative, hydrophobic polysaccharide derivatives can be used to create well-defined nanoparticles from renewable resources.[6–8] One of these derivatives is cellulose acetate (CA), which has been utilized as a bulk material for decades in industry and medicine.[9] It has recently been shown that CA nanoparticles can be synthesized in high yields by a convenient nanoprecipitation method.[7] Since CA is relatively inert, selective chemical modifications are limited.

It is difficult to produce polysaccharide nanoparticles with specific surface functionalities, which is essential in controlling, for example, distributions or cell interactions in vivo.[2,3] In situ prepared functional composite nanoparticles from CA and hydrophilic polysaccharides are a promising alternative. The advantage of this approach is the huge variety of available hydrophilic polysaccharides. Chemical modifications are not required. Composite nanoparticles formed in this way would open new ways to extend the applicability of polysaccharide nanoparticles.

In this work we aimed to combine the nanoparticle forming properties of hydrophobic CA with the properties of four different hydrophilic polysaccharides: hydroxyethyl cellulose (HEC), carboxymethyl cellulose (CMC), low-molecular-weight chitosan (L-CHI), and amino cellulose (AC). These polysaccharides were chosen as they are widely used in nanoparticle preparation and possess great potential to be applied in medicine, the pharmaceutical industry, and bio and food technology.[1–3,5,10–14]

M. R. Kulterer, V. E. Reichel, R. Kargl, Prof. V. Ribitsch
Institute of Chemistry and CePoL
Karl-Franzens University Graz
Nawi Graz, Heinrichstraße 28, AT-8010 Graz, Austria
E-mail: martin.kulterer@uni-graz.at;
volker.ribitsch@uni-graz.at
Dr. S. Köstler
Joanneum Research, Materials
Steyrergasse 17, AT-8010 Graz, Austria
V. Sarbova, Prof. T. Heinze
Institute of Organic Chemistry and Macromolecular Chemistry
Kompetenzzentrum Polysaccharidforschung
Friedrich Schiller University of Jena
Humboldstrasse 10, D-07743 Jena, Germany
Prof. K. Stana-Kleinschek
Laboratory for Characterization and Processing of Polymers
University of Maribor
Smetanova Ulica 17, SI-2000 Maribor, Slovenia

DOI: 10.1002/adfm.201102350

Using these polysaccharides, we generated CA composite nanoparticles with hydroxyl- (HEC), carboxyl-(CMC), and primary and/or secondary amino- (L-CHI, AC) functionalities.

The composite nanoparticles were prepared by precipitating CA into solutions of the aforementioned polysaccharides according to a nanoprecipitation method that has been recently developed by our group.[7] The nanoparticles were synthesized at different pH and hydrophilic polysaccharide content in order to investigate the interactions between CA and the functional polysaccharides. The pH and ionic strength dependent colloidal properties such as particle diameter and effective zeta-potential were determined by dynamic and electrophoretic light scattering (DLS and ELS), whereas the nanoparticle charge was evaluated using polyelectrolyte titration. The morphology of the prepared composite nanoparticles was investigated by scanning electron microscopy (SEM).

As an alternative approach, composite nanoparticles were prepared by adsorbing the functional polysaccharides onto the surface of the CA nanoparticles in a second step after the nanoparticle preparation. This approach is commonly used in the modification of nanoparticles with functional polymers.[1,3]

Finally, the potential of polysaccharide composite nanoparticles for pharmaceutical and bio and food applications was evaluated. In order to show the composite nanoparticles usability for solubilizing and delivery of lipophilic substances in aqueous environment, the particles were loaded with pyrene, a hydrophobic dye, in situ during the nanoparticle formation process. Pyrene also serves as a fluorescence probe for the hydrophobicity of its environment.[15,16] Hence its fluorescence emission spectra provide information about the nanoparticles' structure.

A second applicatory field is to generate selectively functional nanostructured surfaces. The prepared polysaccharide nanocomposites were applied to different polysaccharide surfaces and their influence on the bacterial growth was investigated. Remarkable differences in the surfaces antimicrobial activities were observed, comparing the applied nanostructures with polysaccharide coatings.

The presented work provides, on the one hand, information about the polysaccharide composite nanoparticles' formation processes and properties and, on the other, forms a basis for the utilization of such nanoparticle biocomposites in bio- and life sciences.

2. Results

2.1. Optimization of the In Situ Preparation Method

The size of the CA nanoparticles obtained via nanoprecipitation can be minimized by varying several process parameters, as recently reported.[7] Based on these results, the composite nanoparticles' size was minimized by varying the dispersive media hydrophilic polysaccharide content and pH.

The composite nanoparticles' size and polydispersity index (PdI) were not affected by varying the dispersive media polysaccharide content (15×10^{-4} to 10×10^{-3} wt%). Hence the data are not shown explicitly. All further experiments were conducted with one polysaccharide concentration (15×10^{-4} wt%), in order to minimize the amount of possible unbound polysaccharide.

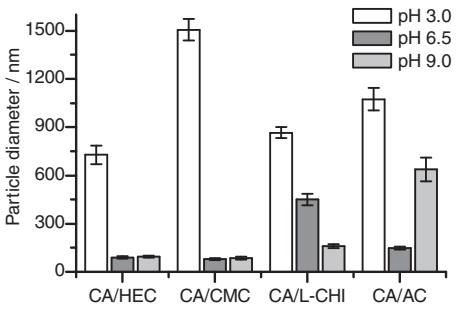

Figure 1. Correlation between mean composite nanoparticle diameter and dispersive media pH.

The pH value of the dispersive media influences the formation of nanoparticles to a high extent (**Figure 1**). Only large aggregates were formed at acidic pH. CA/HEC and CA/CMC nanoparticles were successfully generated at neutral and alkaline pH value. Compared to pH 9.0, smaller CA/AC nanoparticles were generated at pH 6.5, but the smallest CA/L-CHI NPs were obtained at pH 9.0. For all further investigations, CA/HEC, CA/CMC and CA/AC nanoparticles were generated at pH 6.5, whereas CA/L-CHI nanoparticles were prepared at pH 9.0.

2.2. CA Nanoparticle Functionalization via Adsorption

For the purpose of comparison, we attempted to generate composite nanoparticles by adsorbing hydrophilic polysaccharides onto already prepared CA nanoparticles. The adsorption experiments were performed at different polysaccharide contents ($0–75 \times 10^{-4}$ wt%), at pH 2.0–9.0.

The addition of HEC and CMC did not change the nanoparticle characteristics and L-CHI acted as a flocculation agent, regardless of which pH value and polysaccharide concentration ($0–75 \times 10^{-4}$ wt%) was used.

The addition of AC moderately increased the particle size and changed the effective zeta-potential, but did not influence the PdI (15×10^{-4} wt% AC content: mean diameter = 129 nm, PdI: 0.18, effective zeta-potential = +16 mV). However, the particles were very sensitive to changes in pH value and ionic strength and coagulated within one day after preparation. Therefore, the particle properties are not presented in detail.

2.3. Characterization of In Situ Prepared Polysaccharide Composite Nanoparticles

The in situ prepared composite nanoparticles were characterized by DLS (size, PdI), ELS (effective zeta-potential), SEM (shape, size), polyelectrolyte titration (charge), and by determining the nanoparticle yields (**Table 1**).

The mean particle diameter was significantly influenced by the hydrophilic polysaccharides (Table 1). Functionalization with HEC and CMC reduced the particle size (30 nm), whereas the CA/L-CHI and CA/AC nanoparticles were larger (35 nm)

Table 1. Mean diameter, PdI, effective zeta-potential (pH 6.5), and yields of in situ prepared composite nanoparticles.

Nanoparticle	Diameter [nm]	STD [nm]	PdI [nm]	Zeta-potential [mV]	Yield [%]	STD [%]	pK
CA	120	18	0.21	–37	87	12	–
CA/HEC	89	7	0.18	–21	82	9	–
CA/CMC	95	6	0.16	–27	87	12	5.0[11,26]
CA/L-CHI	159	12	0.18	–19	69	11	6.3–6.5[21]
CA/AC	148	9	0.12	+24	71	14	4.5 and 9.0[25]

compared to the non-functionalized CA nanoparticles. The polydispersity indices (PdI) of all the composite nanoparticles (below 0.19) indicate a very narrow size distribution. The yields obtained were high and very similar for all the nanoparticles.

The functionalization of the nanoparticles with hydrophilic polysaccharides led to significant effective zeta-potential shifts (10–61 mV). HEC, CMC, and L-CHI decreased the effective zeta-potential in the order CMC < HEC ≤ L-CHI. The CA/AC nanoparticles provided positive effective zeta-potentials, which were, in absolute values, lower than that of the non-functionalized CA nanoparticles.

SEM images (**Figure 2**) of the composite nanoparticles show spherical shaped nanoparticles. The diameter of the particles increased in the order HEC ≈ CMC < L-CHI ≈ AC. The particle sizes were slightly smaller than that measured with DLS.

Only CMC and AC were highly charged at neutral pH, as examined using polyelectrolyte titrations of the dispersive media. CA/CMC nanoparticles were negatively charged, CA/AC nanoparticles were positively charged and no charges were detected for CA/HEC, CA/L-CHI, and the non-functionalized CA nanoparticles. The results for CMC and AC are shown in **Figure 3**.

The presence of unbound CMC and AC in the nanoparticle suspensions was evaluated by comparing the measured charge before and after dialysis against bidistilled water. The pure polysaccharide solutions' charge decreased below the method's limit of detection during dialysis. In contrast, the differences in charge of the nanoparticle suspensions before and after dialysis are insignificant (Figure 3).

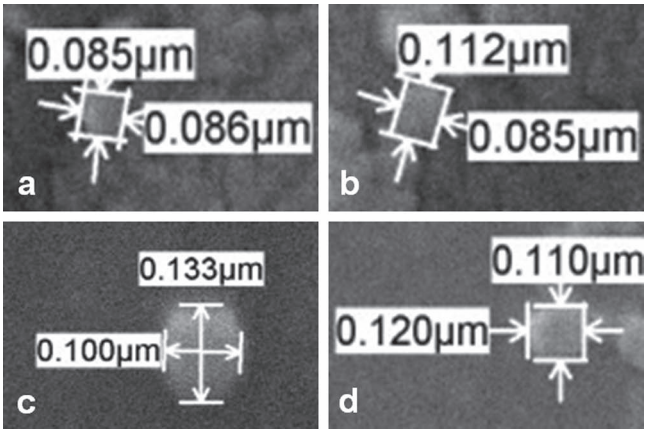

Figure 2. SEM images of in situ prepared composite nanoparticles. a) CA/HEC, b) CA/CMC, c) CA/L-CHI, and d) CA/AC.

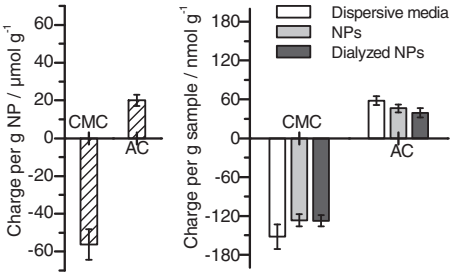

Figure 3. Polyelectrolyte titration results for CA/CMC and CA/AC nanoparticles and the respective polysaccharide solutions. Left: Charge per nanoparticle mass after dialysis. Right: Charge per mass sample before and after dialysis.

2.4. Influence of pH and Ionic Strength on the Nanoparticle Effective Zeta-Potential and Size

The correlation between the effective zeta-potential, the pH value and the ionic strength provides information about the nanoparticles' surface physical and chemical properties.[17–20] The effective zeta-potential was measured at pH 3.0–9.0, and at varying ionic strengths (0–150 mM NaCl, pH 6.5).

The pH dependent zeta-potential is depicted in **Figure 4**. The effective zeta-potential of CA/HEC nanoparticles decreased towards low pH (from –25 mV to –5 mV). The effective zeta-potential of the CA/CMC nanoparticles was constant from pH 5.0 to 9.0 (–28 mV). Below pH 5, their effective zeta potential decreased linearly towards lower pH (from –28 mV to –5 mV). The CA/L-CHI nanoparticles comprised negative effective zeta-potentials under neutral and alkaline conditions, which decreased (by 10 mV) towards lower pH. From pH 6.0–5.0 the effective zeta-potential increases to a positive plateau level (+20 mV), which was constant at acidic pH. The values obtained for the CA/AC nanoparticles were positive over the pH range investigated, decreased slightly from pH 3.0–8.0, and dropped from pH 8.0–9.0 (by 14 mV).

The correlation between the composite nanoparticles' effective zeta-potential and ionic strength is depicted in **Figure 5**. The absolute values of the CA/AC, CA/CMC and non-functionalized

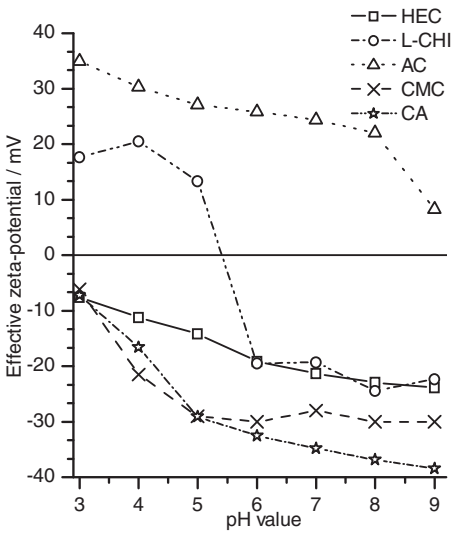

Figure 4. pH-dependent effective zeta-potential of composite nanoparticles prepared in situ.

CA nanoparticles decreased strongly with increasing ionic strength from 0–10 mM. In contrast, the effective zeta-potentials of the CA/HEC and CA/L-CHI nanoparticles did not change significantly. The values of all the particles approached plateau levels with further increased ionic strengths. The plateau levels of the CA/HEC, CA/L-CHI, CA/CMC, and non-functionalized CA nanoparticles were very similar (≈ –5 mV). In contrast, the plateau level of the CA/AC nanoparticles was positive and higher (by 22 mV) than that of the non-functionalized CA nanoparticles.

The nanoparticles' stabilities were influenced by the pH values of the suspensions as well as by the ionic strength. The diameters of the CA/HEC, CA/CMC, and non-functionalized CA nanoparticles[7] were constant at alkaline and neutral pHs, but started to increase below pH 4.0. The CA/L-CHI nanoparticles were stable at alkaline as well as acidic pHs, but coagulated between pH 4.0–5.0. The CA/AC nanoparticles coagulated above pH 9.0. The size of all the investigated nanoparticles started to increase at suspension ionic strengths above 5 mM. All the nanoparticle suspensions were stable and did not sediment below 125 mM.

2.5. Stability of Composite Nanoparticles

The composite nanoparticles' stability against mechanical stress (centrifugation and redispersion) and during storage is important if the aim is to evaluate the particles' usability for a designated application. Additionally, the nanoparticles' stability reflects their surface properties.

The centrifugation (time, centrifugal force) and redispersion (sonication time) conditions were optimized in order to find the optimal balance between efficient sedimentation and redispersibility (data not shown explicitly). The diameter of CA/HEC nanoparticles (67 nm) and CA/CMC nanoparticles (38 nm) increased significantly. The mechanical stress did not lead to a significant increase of the CA/AC nanoparticles' size. It was not possible to redisperse non-functionalized and CA/L-CHI nanoparticles.

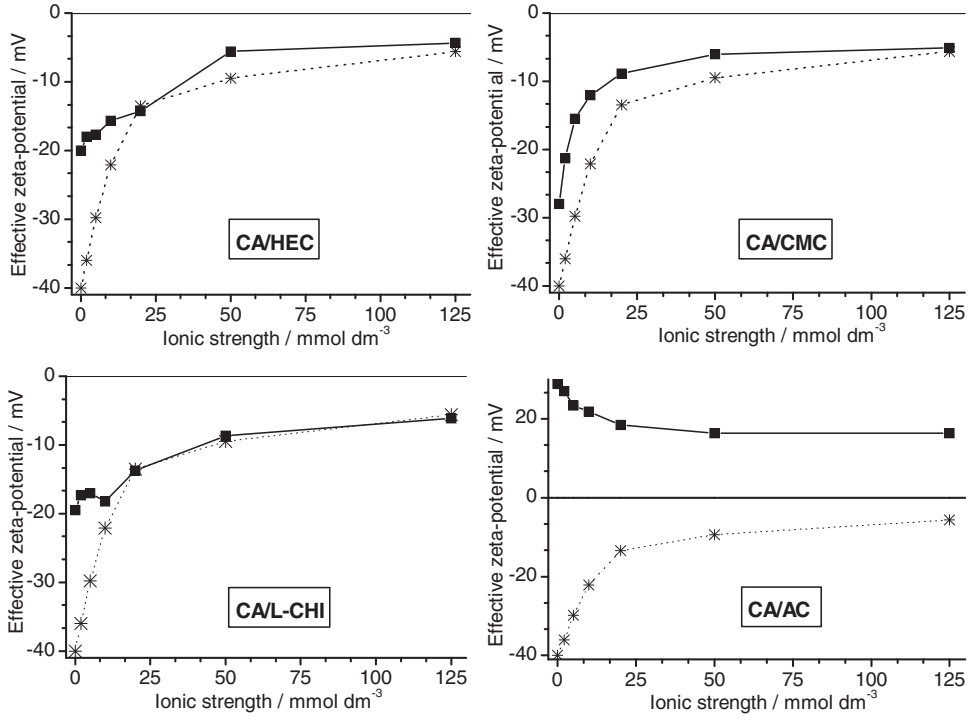

Figure 5. Effective zeta-potential of in situ prepared composite nanoparticles with respect to the suspensions' ionic strength. Dotted line: non-functionalized CA nanoparticles.

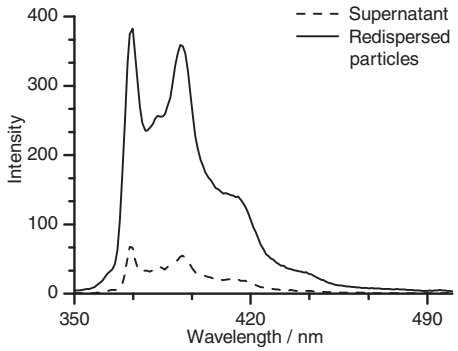

Figure 6. Fluorescence spectra of pyrene encapsulated into CA/CMC nanoparticles.

The long term stability of composite nanoparticles was evaluated by monitoring the particle size during storage for 28 days. The diameter of the CA/L-CHI (64 nm) and non-modified CA nanoparticles (25 nm) increased over time. The CA/HEC, CA/CMC and CA/AC nanoparticles' size did not change significantly.

2.6. Encapsulation of Pyrene

CA nanoparticles allow the release of entrapped drugs over time in a controlled manner.[8] In order to evaluate the potential of CA composite nanoparticles for these purposes, pyrene (a hydrophobic fluorescent dye) was entrapped into CA/CMC nanoparticles in situ during the nanoparticle formation process. The nanoparticles were separated from the solution and the maximum intensity of the sedimented/redispersed nanoparticles was greater than that of the supernatant by a factor of four (**Figure 6**).

2.7. Nanostructuring of Surfaces and Antimicrobial Properties

Another applicatory field of interest is the specific design of nanostructures on surfaces. This was evidenced by applying composite nanoparticles onto different polysaccharide surfaces. Moreover, the composite nanoparticles' adsorption behavior reflects their surface properties.

Composite nanoparticles were applied to HEC, CMC, or L-CHI coated SEM object holders. The CA/HEC and CA/CMC nanoparticles adsorbed only on L-CHI. The CA/L-CHI nanoparticles adsorbed on CMC, but not on HEC or L-CHI. Considerable amounts of CA/AC nanoparticles were found only on the CMC coated supports. All the composite particles adsorbed in the form of a single layer of uniformly distributed, individual nanoparticles (**Figure 7**).

Applying composite nanoparticles allows new functions to be introduced to a surface. This was demonstrated by the selective tuning of the surfaces' antimicrobial properties. In particular, bacterial growth (*Escherichia coli* MG1655 [R1-16]) was evaluated on the CMC surfaces before and after applying CA/L-CHI nanoparticles, and on the L-CHI surfaces before and after coating with CA/CMC nanoparticles. CMC does not inhibit bacterial growth, whereas chitosan is known to provide

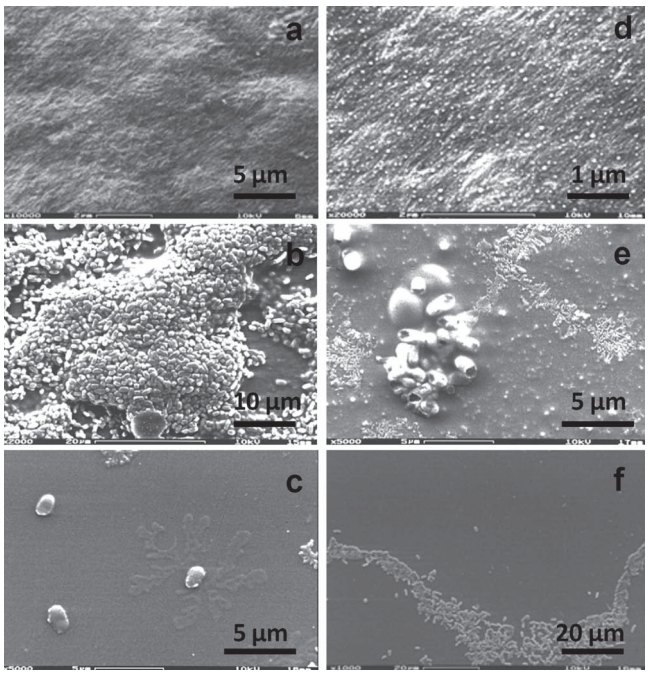

Figure 7. Bacterial growth on plain and nanostructured polysaccharide surfaces. a) Polysaccharide surface (CMC), b) bacterial growth on CMC, c) bacterial growth on L-CHI. d) CA/CMC nanoparticles on L-CHI, e) bacterial growth on CA/L-CHI nanoparticles, and f) bacterial growth on CA/CMC nanoparticles decorated L-CHI.

antimicrobial properties.[14,21] Bacteria grew densely on the CMC surfaces (Figure 7b) forming an early stage biofilm.[22] On the CA/L-CHI nanoparticle coated CMC surfaces (Figure 7e) only a few, abnormally shaped bacteria were found. Analogous to this, a few single bacteria surrounded by a flower-like structure (Figure 7c) were found on the L-CHI surfaces. On the CA/CMC nanoparticle coated chitosan surfaces, bacteria showed regular growth behavior (Figure 7f).

Additionally, the influence of the applied coatings on the amount of bacteria growing in the suspensions after incubating three days was investigated by measuring the OD_{600} (the suspension's optical density at a wavelength of 600 nm; an OD_{600} = 1 equates to 10^9 bacteria in 1 mL suspension). The bacteria in suspension were able to grow nicely in presence of CA/CMC nanoparticles coated substrates ($OD_{600} = 2.46 \pm 0.45$). This was also observed for CMC surfaces ($OD_{600} = 2.71 \pm 0.21$). The number of bacteria found in suspensions in contact with L-CHI surfaces was significant lower ($OD_{600} = 0.69 \pm 0.07$). The lowest number of bacteria was found in suspensions in contact with CA/L-CHI nanoparticles decorated substrates ($OD_{600} = 0.36 \pm 0.18$).

3. Discussion

3.1. Preparation of Polysaccharide Nanoparticles: Comparison of Preparation Techniques

CA nanoparticles were successfully in situ functionalized with HEC, CMC, L-CHI, and AC, as demonstrated by the different

nanoparticle sizes, effective zeta-potentials, and charges (Table 1, Figure 2,3). The data are supported by the changes in the nanoparticle stabilities, adsorption behaviors, and antimicrobial properties (Figure 7). SEM showed particles that were slightly smaller than the mean particle diameter (DLS), but DLS gave the mean hydrodynamic diameter, whereas SEM showed single, vacuum-dried nanoparticles.

One aim of this study was to gain information about the hydrophilic polysaccharides' role in the in situ nanoparticle preparation process. A possible scenario is the adsorption of polysaccharides after nanoparticle precipitation. The diameters of in situ prepared composite nanoparticles differ strongly from non-functionalized CA nanoparticles (Table 1). The relatively large particle sizes of the CA/L-CHI and CA/AC nanoparticles cannot be explained by polysaccharide adsorption. The particles are not coagulated, as evidenced by their low PdI (which indicates a narrow size distribution) and SEM images (Figure 7). Moreover, the small diameter of the CA/HEC and CA/CMC nanoparticles indicates that the polysaccharides are involved in the particle formation process. For a better comparison, the polysaccharides were adsorbed onto already prepared CA nanoparticles. Only AC bound to the CA nanoparticles, but the CA/AC nanoparticles prepared in this way were highly instable.

In summary, the in situ method of preparing composite nanoparticles allows the binding of hydrophilic polysaccharides that do not adsorb onto CA (HEC, CMC, L-CHI). The mean particle diameter varies to a large extent, which is not the case when polysaccharides are adsorbed onto already prepared CA nanoparticles. Accordingly, in situ prepared CA/AC nanoparticles are much more stable than particles prepared via adsorption. This provides evidence that the hydrophilic polysaccharides are involved in the particle formation process; they are incorporated into the CA nanoparticle matrix yielding stable composite nanoparticles.

3.2. Role of Hydrophilic Polysaccharides in the In Situ Nanoparticle Formation Process

The formation of CA nanoparticles can be regulated by adjusting the dispersion and diffusion of the CA solution into the dispersive media. The nanoparticles are finally formed by the water (non-solvent) driven phase separation of CA and its liquid surrounding.[7]

The hydrophilic polysaccharides are involved in this process, and therefore impact the nanoparticles' size and surface properties (Table 1). The dispersive media pH affects the particle formation process to a large extent because it influences the interactions between CA, hydrophilic polysaccharide, and the solvents[7,23] (Figure 1). Moreover, one has to be aware that, in addition to electrostatic and hydrophilic interactions, hydrophilic polysaccharides also comprise hydrophobic moieties and can, therefore, act as dispersing agents.[24]

The relatively small diameter of CA/HEC and CA/CMC composite nanoparticles obtained at neutral and alkaline pH can be explained by this dispersing effect. HEC and CMC bind to newly formed particle walls due to hydrophobic interactions. These walls are then separated from each other because of the acquired negative potential and a strongly bound layer of water molecules (Figure 4). The potential of the polymers is almost zero at around pH 2.0 and the repulsing forces are therefore suppressed. This causes increased particle sizes in status nascendi.

L-CHI act, when positively charged (at pH 2.0),[21,25] as a flocculent. At pH 9.0, the molecules are more hydrophobic.[23] Their potential is negative (similar to HEC, Figure 4) because its amino functions are not protonated and hydrated OH^- ions are adsorbed. Therefore L-CHI acts as a dispersing agent, resulting in smaller particles.

AC displayed less distinctive behavior. In contrast to the other soluble PS, it has a strong affinity to non-functionalized CA nanoparticles. The balance between the dispersive attraction forces and the electrostatic forces needs further investigation.

Based on our findings, we propose the following functionalization mechanism. The hydrophilic polysaccharides most probably diffuse (together with water molecules) into CA-rich domains. They concentrate at the surface of these domains because of hydrophobic interactions[24] and act as dispersing agents due to electrosteric interactions. Finally, the hydrophilic polysaccharides become entrapped into the CA nanoparticle matrix during the phase separation. This yields functional composite nanoparticles with hydrophobic domains and hydrophilic surfaces, as shown by the fluorescence emission spectra of the encapsulated pyrene and effective zeta-potential measurements.

3.3. Surface Properties of In Situ Prepared Composite Nanoparticles: Charge and Zeta-Potential

The particle charges were evaluated by polyelectrolyte titration, assuming a 1:1 stoichiometry between the analyte and an oppositely charged titrant.[17,26] The method provides useful qualitative and semiquantitative information about the charge of a sample (especially when comparing samples of similar nature). Functionalization with charged CMC and AC yields charged nanoparticles (at neutral pH), which demonstrates the successful functionalization of uncharged CA nanoparticles. The higher charge of CA/CMC compared to CA/AC nanoparticles is presumably attributable to the differences in the polysaccharides' degree of substitution (DS_{CMC}: 1.27, DS_{AC}: 0.75) (Figure 2). The particle suspensions' charges before and after dialysis was measured in order to estimate the amount of unbound polysaccharide (Figure 2). Since the charge differences are insignificant, the majority of CMC and AC are bound to the nanoparticle matrix.

The effective zeta-potential as a function of the pH reflects the nanoparticles' surface charge density and hydrophilicity. The nanoparticles' effective zeta-potential origins from dissociable functional groups and from adsorbed ions.[17–20]

Non-modified CA nanoparticles as well as CA/HEC and CA/L-CHI nanoparticles are not charged at neutral pH. However, their effective zeta-potential is negative because hydrated OH^- ions adsorb onto their surface.[17] The effective zeta-potential of CA/CMC nanoparticles is more negative than that of CA/HEC and CA/L-CHI nanoparticles because of the presence of negatively charged carboxylic groups. Analogous to this, CA/AC nanoparticles have positive effective zeta-potentials because they carry protonated amino groups. The functionalization with hydrophilic polysaccharides also increased the

surface hydrophilicity. Hydrophilic polymer surfaces bind water molecules and tend to swell, resulting in lower effective zeta-potentials.[17] Therefore, the absolute zeta-potential of all four composite nanoparticles is lower than that of non-modified CA particles (Table 1).

Because of these effects, nanoparticle functionalization affects the effective zeta-potential pH functions to a high extent (Figure 4). The function of CA/HEC nanoparticles is typical of uncharged hydrophilic nanoparticles. Decreasing the pH decreases the number of adsorbed hydrated OH^- ions and increases the suspensions' ionic strength.[17] This leads to a linear decrease in the effective zeta-potential. The pH dependent effective zeta-potential of CA/CMC nanoparticles is characteristic of charged particles. The plateau at neutral and alkaline pHs can be attributed to fully dissociated carboxylic-groups (pK = 5.5). Below pH 5 the effective zeta-potential decreases because the carboxylic functions become protonated. The function of CA/L-CHI nanoparticles is almost identical to that of uncharged CA/HEC nanoparticles at neutral and alkaline pHs. Below pH 6.0 (pK = 6.3–6.5) the amino groups of chitosan are protonated, yielding a positive effective zeta-potential plateau. CA/AC nanoparticles show positive effective zeta-potentials at pH 3.0 because all amino-groups are protonated (pK_1 = 4.5 and pK_2 = 9). The values decrease with increasing pH because the nanoparticles' charge density decreases.

Investigating the correlation between the effective zeta-potential and the nanoparticle suspensions' ionic strength (Figure 5) provides additional information about the particle surface functionality and structure.[17–20] Oppositely charged ions shield the nanoparticles' surface charge. Hence, an increased ionic strength reduces the effective zeta-potential.[17] Therefore, charged CA/CMC and CA/AC nanoparticles are more sensitive to variations in ionic strength than CA/HEC and CA/L-CHI nanoparticles. The effective zeta-potential approaches a plateau level at high ionic strength, which is characteristic of the nanoparticles' morphology.[17–20] All the composite nanoparticles displayed plateau levels different from zero zeta-potential (Figure 5), which is typical of soft, permeable surfaces.[19] Moreover, the plateau levels of the CA/HEC, CA/L-CHI, CA/CMC, and non-functionalized CA nanoparticles did not differ significantly, indicating a similar surface structure. On the contrary, the CA/AC nanoparticles displayed a different surface morphology since their plateau level was significantly higher.

Therefore, one can suggest that HEC, CMC, and L-CHI form a composite with CA at the particle surface, whereas AC forms a separated surface layer. For particles with soft surfaces, it would be more appropriate to use the electrophoretic mobility instead of the zeta-potential. However, for a better comparison with literature we used the so called "effective" zeta-potential calculated from the Smoluchowski equation.[18]

3.4. Stability of Composite Nanoparticles

Nanoparticles are mainly stabilized via electrostatic forces (charge density) and steric repulsion (polymer structure, swelling, hydrophilicity). The composite nanoparticles' stability was evaluated over a broad pH and ionic strength range as well as during storage and processing (mechanical stress).

A reduced electrostatic stabilization (by changing the pH or increasing the ionic strength) is reflected by low effective zeta-potentials.[17] Composite and non-functionalized CA nanoparticles tend to coagulate at absolute effective zeta-potentials below 15 mV. This demonstrates that electrostatic forces are important to nanoparticle stability.

The CA/HEC and non-functionalized CA nanoparticles coagulated at acidic pH due to the low number of adsorbed hydrated OH^- ions. Accordingly, CA/CMC nanoparticles are not charged and coagulated at low pH. In contrast, CA/AC nanoparticles are charged and therefore stable at acidic pH. The particles coagulated at alkaline pH, where the amino functions are not protonated. CA/L-CHI nanoparticles are stabilized at pHs below 4.0 (protonated amino groups) and at neutral to alkaline pH (adsorption of hydrated OH^- ions). Between pH 4.0 and 5.0 the particles coagulate because almost no electrostatic repulsion is given.

The CA/HEC, CA/CMC, and CA/AC nanoparticles were seen to be highly stable under mechanical stress (centrifugation and redispersion) and during storage compared to the CA/L-CHI and non-functionalized CA nanoparticles. The CA/AC nanoparticles, although less charged (Figure 3), were more resistant to mechanical stress than the CA/CMC nanoparticles. This can be explained by the higher degree of steric repulsion in the CA/AC nanoparticles. The CA/L-CHI nanoparticles were more unstable during storage than the unmodified CA NPs. Hence, electrostatic and steric repulsion are too low to stabilize the particles efficiently.

3.5. Encapsulation of Hydrophobic Substances

One important application for polysaccharide nanoparticles is the solubilization, delivery and release of hydrophobic substances in aqueous environments.[1,8]

In order to show the in situ preparation methods' usability for such applications, pyrene (a hydrophobic fluorescent dye) was encapsulated into the CA/CMC nanoparticles. The encapsulation efficiency was high, since 75% of the pyrene was located in the particles (Figure 6). Therefore, by using this method CA nanoparticles can be functionalized and loaded in one step.

The data provide additional information about the local environment of pyrene. In particular, the third vibrational band intensities increase with increasing hydrophobicity of the surroundings.[15,16] The relative intensities I_1/I_3 therefore reflect the polarity of the molecules' local environment, and can be used to evaluate the distribution of pyrene in the system. The I_1/I_3 value of the centrifuged and redispersed nanoparticles (I_1/I_3:1.49) was much lower than that of pyrene dissolved in water (I_1/I_3:1.76, calculated from Nakajima et al.).[27] Hence, the pyrene was localized in the CA matrix of the nanoparticles (hydrophobic environment), which does not contain considerable amounts of polar molecules (water, hydrophilic polysaccharide). This indicates that the nanoparticles comprise CA domains that are not swollen and do not contain hydrophilic polysaccharides.

3.6. Nanostructuring of Surfaces and Antibacterial Properties

Another applicatory field of interest is the specific design of functional nanostructures on surfaces. In order to evaluate the

adsorption behavior, the composite nanoparticles were applied to different polysaccharide surfaces (Figure 7).

The experiments demonstrated that composite nanoparticles can be used for the selective nanostructuring of polysaccharide surfaces. The composite nanoparticles form a regularly distributed layer of individualized particles on the polysaccharide surfaces. The nanoparticles showed specific adsorption behavior, which could be attributed to electrostatic and steric interactions. However, further studies are required to understand these processes in detail. The nanoparticle coating, compared to immobilized polymer layers or chemical surface modifications, does not change the surface properties completely. The subjected layer is not densely covered with nanoparticles, and therefore still contributes to the surface properties and is accessible to chemical or physical modifications.

By applying such nanostructures, it is possible to tune the antimicrobial properties of the polysaccharide surface. The nanoparticles influence the ability of bacteria to grow and attach to the surface. This can be seen by comparing the bacterial growth (Figure 7). Only a few bacteria were found on the L-CHI surfaces and on the CA/L-CHI nanoparticles coated CMC surfaces. These bacteria were dead since they were highly deformed. Cytoplasm was spread around the dead bacteria (flower-like structure) showing that the cell walls had been destroyed. However, more bacteria and bacterial compartments were found on the CA/L-CHI nanoparticle coated CMC surfaces. These surfaces also provide CMC domains between the nanoparticles. Therefore, parts of the cells which do not bind to L-CHI can attach to the surface. Moreover, a nanoparticle coating increases the surface roughness, which encourages the adsorption of bacteria and cell fragments.[28] On CMC surfaces the bacterial growth was not hindered, and the bacteria formed an early stage biofilm. Bacteria also grew on the CA/CMC coated L-CHI surfaces, but not as dense as on plain CMC surfaces. The surface provides CMC domains where parts of the cells can attach. Moreover, the increased surface roughness may also encourage the adoption of cell compartments. This suggests that non-coated L-CHI domains have a negative effect on bacteria and hamper their growth.

In addition, the influence of the nanocoating on the bacterial growth in the surrounding was investigated by evaluating the amount of bacteria in the suspension (measuring the OD_{600}). No significant difference was observed between CA/CMC nanoparticle coatings and CMC surfaces, showing that in both cases CMC dominates the interactions of the surface with bacteria. L-CHI surfaces reduced the bacterial growth in suspension by a factor of four compared to CMC surfaces. Most interestingly, the antimicrobial activity of loosely packed CA/L-CHI nanoparticles was by a factor of two stronger compared to L-CHI surfaces. This could be explained by a better contact of the bacteria with L-CHI, on the one hand because of an increased accessible surface, and on the other hand by an increased surface roughness. However, also the structure of the L-CHI molecules at the surface can affect the antimicrobial activity, and further studies are required to understand these effects in detail.

4. Conclusions

With this work we were able to show how composite nanoparticles of CA and different water soluble polysaccharides can be prepared. Applying an easy-to-use co-nanoprecipitation technique we were able to selectively tune the composite nanoparticles properties. The integration of different polysaccharides such as HEC, CMC, L-CHI, and AC enabled the formation of composite nanoparticles with different sizes, charges, and effective zeta-potentials. Hence, the hydrophilic polysaccharides bind to the CA nanoparticle matrix during the precipitation process and determine their surface characteristics.

The CA nanoparticle functionalization also improved the nanoparticles' stability, specified their adsorption behavior and introduced antimicrobial properties.

In addition, the adsorption of polysaccharides onto already precipitated CA nanoparticles was tested, in order to gain information about the composite nanoparticles' formation mechanism. Based on these results, the conclusion can be made that adsorption on its own does not lead to the formation of stable composite nanoparticles. The polysaccharides are incorporated into the CA matrix during the precipitation process and another mechanism has to be of importance considering the co-precipitation mechanism. However, the hydrophilic polysaccharides are concentrated at the nanoparticle surface (effective zeta-potentials). Additionally, it was shown that the nanoparticles are composed of hydrophobic domains that do not contain considerable amounts of water or hydrophilic polysaccharides (fluorescence data of encapsulated pyrene).

More information about the composite nanoparticles formation mechanism is provided by the nanoprecipitation experiments at different pHs. The pH affects the polysaccharides' potential and hydrophilicity, and hence influences the interactions of polysaccharides, CA, and solvent molecules.

We suggest that the hydrophilic polysaccharides (which are also composed of hydrophobic domains) act similarly to dispersive agents. They become concentrated at the boundary between the CA-rich domains and the surrounding solution and separate these domains due to electrosteric repulsion. Finally, the functional polysaccharides are incorporated into the CA nanoparticle matrix when phase separation occurs.

The functional composite nanoparticles exhibit great potential to be used in the solubilization and delivery of hydrophobic substances in aqueous systems. This was demonstrated by the successful entrapment of pyrene (a hydrophobic fluorescent dye) into CA/CMC nanoparticles and the specific adsorption of these nanoparticles onto polysaccharide surfaces. The second applicatory field of interest is the design of functional nanostructures onto different polysaccharide surfaces, which was evidenced by applying monolayer of individual CA/L-CHI nanoparticles that provide stronger antimicrobial activity than plain L-CHI surfaces.

5. Experimental Section

Materials: All analytical grade chemicals were used as obtained. Tetrahydrofuran (THF) and sodium monochloroacetate were purchased from Merck (Darmstadt, Germany). Ethylene diamine, acetic acid, cellulose acetate (CA, 39.8 wt% acetyl content, DS 2.5, M_n = 30 000 g mol^{-1}), poly(sodium4-styrenesulfonate) (PES, M_w=70000 g mol^{-1}), and poly(diallyldimethyl-ammonium chloride) (polyDADMAC M_w 300 000 g mol^{-1} to 500 000 g mol^{-1}, 20 wt% aqueous solution) were purchased from Sigma-Aldrich (Steinheim, Germany). Hydroxyethyl cellulose (HEC,

viscosity of a 1 wt% solution in H_2O at 20 °C: 145 mPa s) and pyrene were purchased from Fluka (Buchs, Switzerland). Acetone, methanol, ethanol, 2-propanol, isopropanol, dimethyl sulfoxide (DMSO), sodium chloride (NaCl), potassium, chloride (KCl), monopotassium phosphate (KH_2PO_4), disodium hydrogen phosphate (Na_2HPO_4), hydrochloric acid ((HCl) 37 wt% aqueous solution), and sodium hydroxide (NaOH) were purchased from Roth (Karlsruhe, Germany). Low molecular weight chitosan was prepared according to the method of Fasl et al.[29] Spectra/Por CE dialysis tubings with a 100 kDa molecular weight cut-off (MWCO) and 10 mm flat width were purchased from Spectrum Laboratories Inc. (Breda, Netherlands). A three blade stirrer R 1381 (diameter: 45 mm, ID-Nr.: 1296000) was purchased from IKA–Werke GMBH & CO. KG (Staufen, Germany). Tosyl cellulose (DS 0.87) was kindly provided by the Thüringisches Institut für Textil-und Kunststoff-Forschung e.V. ((TITK) Rudolstadt, Germany).

Synthesis of Water Soluble Amino Cellulose (AC): Tosyl cellulose (180 g, DS 0.87) was dissolved in DMSO (1.8 L) overnight. Ethylene diamine (950 mL) was added and the reaction mixture was allowed to react under stirring (100 °C, 6h). The product was precipitated in a mixture of acetone/2-propanol (50/50) and washed with 2-propanol four times to remove possible byproducts. After drying in a vacuum (40 °C), 6-deoxy-6-ethylenediamino cellulose (110 g) was obtained. The product was light-yellow colored and soluble in water. The degree of substitution-values (DS) was determined by elemental analysis. The DS of amino-functions was 0.75 (N-content: 9.78 wt%), and the DS of the remaining tosyl moieties was 0.1 (S-content: 1.60 wt%). An M_n of 23 300 g mol^{-1} was determined by gel permeation chromatography (GPC) (data not shown explicitly).

Synthesis of Carboxymethyl Cellulose (CMC): Cellulose (5.0 g) was slurried in isopropanol (150 mL). After the addition of aqueous NaOH (15% w/v, 13.3 mL), stirring continued for 1 h at room temperature. Sodium monochloroacetate (7.2 g) was added and the mixture was allowed to react under stirring (5 h, 55 °C). The product was filtered off, dispersed in aqueous methanol (80% v/v) and neutralized with acetic acid. Impurities were removed by washing with aqueous ethanol (80% v/v, 3×) and ethanol, and the product was dried in a vacuum (60 °C) to yield 8.4 g. The DS was 1.28, as determined by ^{1}H-NMR spectroscopy after hydrolytic chain degradation according to a published procedure,[30] and the degree of polymerization (DP) was 574, as obtained from GPC measurements (data not shown explicitly).

Preparation of Polysaccharide Composite Nanoparticles: The in situ preparation was performed according to a nanoprecipitation method previously reported by our group.[7] Typically, CA (20 mg) was dissolved in THF (10 mL). The CA solution was added dropwise to aqueous polysaccharide solution (60 mL, 15×10^{-4} wt% HEC, CMC, L-CHI or AC) under sonication and continuous stirring (three blade stirrer, 350 rpm). The dispersive media pH was adjusted to pH 6.5 for HEC, CMC, and AC, and to pH 9 for L-CHI. Non-functionalized CA nanoparticles were prepared with bidistilled water as the dispersive media. The final nanoparticle suspensions were filtered (5 µm polytetrafluoroethylene (PTFE) syringe filter) to remove large coagulates. THF was removed by stirring the nanoparticle suspensions in a continuous nitrogen flow overnight at room temperature. The yields were determined by comparison of the nanoparticle mass with the initial amount of CA and the hydrophilic polysaccharide. The nanoparticle mass was measured via gravimetrical analysis of the filtrated and lyophilized nanoparticle suspensions.

CA/CMC nanoparticles prepared in this way were labeled in situ with pyrene in order to show their potential for the encapsulation and delivery of hydrophobic substances. Typically, a pyrene solution (in THF) was added to the CA solution prior to nanoprecipitation (pyrene content in nanoparticle suspension: 0.24 µM). The encapsulation efficiency was evaluated by separating the nanoparticles from the solution and comparing the fluorescence emission intensities. Typically, the nanoparticle suspension was centrifuged (10 min, 6300 rcf) and the supernatant was separated from the pellet (it was not possible to separate the nanoparticles quantitatively). The pellet was then washed five times and redispersed in bidistilled water by intense shaking and sonication. The fluorescence emission spectra (excitation wavelength: 305 nm) were measured using a Perkin Elmer Luminescence Spectrometer LS 50B. All experiments were performed in triplicate.

For comparison, CA nanoparticles were functionalized by the adsorption of hydrophilic polysaccharides. Typically, a certain amount (between 8 µL and 300 µL) of a aqueous polysaccharide solution (30×10^{-3} wt% HEC, CMC, L-CHI, or AC) was added to a 1:2 diluted CA nanoparticle suspension (12 mL, continuous stirring). After addition of the polysaccharide, the nanoparticle suspensions were stirred for 30 min. The influence of pH on the adsorption process was investigated by varying the dispersive media's pH (pH 3, pH 6.5, and pH 9). All experiments were done three times.

Dynamic and Electrophoretic Light Scattering: The nanoparticles' mean hydrodynamic diameter and polydispersity indices (PdI) were determined by dynamic light scattering (DLS) using a Brookhaven Instruments ZetaPlus zeta-potential Analyzer (wavelength: 674 nm, scattering angle: 90°). The samples were diluted with bidistilled water (10×10^{-3} wt% particle content). Mean particle diameters were approximated as the effective (z-average) diameters. The width of the distribution and the PdI were achieved using the cumulants method, presuming spherical particle shape and log-normal size distribution. The measurements were repeated five times for each sample.

The nanoparticles' effective zeta-potential[18] was measured by electrophoretic light scattering (ELS) using a Brookhaven Instruments ZetaPlus zeta-potential Analyzer in PALS (wavelength: 674 nm). The samples were diluted with bidistilled water (10×10^{-3} wt% particle content). The effective zeta-potential was calculated using the Smoluchowski equation.[17–19] The measurements were repeated five times for each sample. The intrinsic error of the measured zeta-potential was ±5 mV.

The effect of pH and ionic strength on the mean nanoparticle diameter and effective zeta-potential was analyzed for suspensions pH 3.0–10.0 and NaCl content 0–150 mM.

Polyelectrolyte Titration: The nanoparticle surface charge was determined by polyelectrolyte titration.[17,26] All titrations were performed in triplicate using an AFG Analytic GMbH Charge analyzing system. Typically, the charge of a sample solution (10.0 g, pH 6.5, room temperature) was determined by titration against aqueous PES (0.5 mN, to determine a positive charge), or polyDADMAC (0.5 mN, to determine a negative charge). The charge per gram of nanoparticle was calculated from process yields (Table 1).

The amount of unbound polysaccharides that might be present in the composite nanoparticle suspensions was evaluated by removing the unbound polysaccharides via dialysis and comparing the measured charges before and after dialysis. Typically, samples were dialyzed against bidistilled water (72 h, changing the water reservoir every 12 h) at room temperature.

Nanoparticle Stabilities During Storage and Sedimentation/Redispersion: In order to investigate the stability of the composite nanoparticle suspensions over time, the particle sizes were monitored over four weeks. The nanoparticles were stored at room temperature.

The influence of mechanical stress and compaction on the nanoparticle sizes was investigated by measuring the particle diameter before and after sedimentation and redispersion. Typically, a nanoparticle suspension (10 mL) was centrifuged (10 min, 12 200 rcf for CA/HEC and CA/AC nanoparticles, 10 min, 6300 rcf for CA/CMC nanoparticles) using an Eppendorf Centrifuge 5804 R. The precipitate was separated from the supernatant and rinsed with bidistilled water five times. The pellet was redispersed in bidistilled water (10 mL) by intense shaking and sonication (10 min). The mean particle diameter was measured with DLS. All experiments were performed in triplicate.

Evaluation of the Nanoparticle Shape, Adsorption Behavior, and Antimicrobial Properties (SEM, Optical Density OD): To analyze the nanoparticle shape, the composite nanoparticles were immobilized on carbon-coated SEM sample holders. A 1:5 diluted nanoparticle suspension (500 µL) was placed on the object holder, and the sample was then dried under reduced pressure.

In order to evaluate the adsorption properties of the composite nanoparticles, carbon coated sample holders were coated with CMC,

L-CHI or HEC via dip coating. In particular, the sample holders were incubated in aqueous polysaccharide solutions (0.1 wt% polysaccharide, 150 mM NaCl, 1 h) and then washed with bidistilled water two times. The success of the surface modification was evaluated via water contact angle measurements (data not shown explicitly). The composite nanoparticles were applied to the modified sample holders by incubation in 1:5 diluted nanoparticle suspensions (1 h), followed by washing with bidistilled water two times.

These nanostructured surfaces were used to investigate bacterial growth on the composite nanoparticles. The number of bacterial growth in suspension was determined my measuring the optical density at a wavelength of 600 nm (OD_{600}), and the bacterial growth on solid samples was evaluated via SEM.

The OD_{600} was measured using a Hitachi U-5100 photometer. In the case of high bacteria contents ($OD_{600} > 0.8$), the suspensions were diluted 1:5 with the minimal media, and the OD of pure suspensions was then back-calculated using the dilution factor.

The solid samples were incubated in a bacteria suspension of *Escherichia coli* MG 1655 [R1-16] cells (start-OD_{600} = 0.03) for three days. The surfaces were then analyzed using SEM, after extensively washing with buffer (13.7 mM NaCl, 0.27 mM KCl, 10 mM Na_2HPO_4, 0.2 mM KH_2PO_4; pH 7.4) and drying (24 h, room temperature, sterile conditions).

Prior to SEM, the sample holders were sputtered with gold/platinum. For sputtering, a Jeol JFC-1100 E ion sputter was used (D = 10 mA). The thickness of the gold was about 150 Å. A Carl Zeiss FE-SEM SUPRA 35 VP electron microscope was used for the measurements (acceleration voltage: 10 kV).

Acknowledgements

The research leading to these results has received funding from the European Union Seventh Framework Programme (FP7/2007-2013) under grant agreement n° 214653.

Received: September 30, 2011
Published online: February 7, 2012

[1] S. Boddohi, M. J. Kipper, *Adv. Mater.* **2010**, *22*, 2998.
[2] Z. Liu, Y. Jiao, Y. Wang, C. Zhou, Z. Zhang, *Adv. Drug Delivery Rev.* **2008**, *60*, 1650.
[3] C. Lemarchand, R. Gref, P. Couvreur, *Eur. J. Pharm. Biopharm.* **2004**, *58*, 327.
[4] T. Heinze, S. Hornig, *Polysaccharide Mater.* **2009**, *1017*, 169.
[5] T. Heinze, *Macromol. Symp.* **2009**, *280*, 15.
[6] S. Hornig, T. Heinze, *Biomacromolecules* **2008**, *9*, 1487.
[7] M. R. Kulterer, M. Reischl, V. E. Reichel, S. Hribernik, M. Wu, S. Köstler, R. Kargl, V. Ribitsch, *Colloids Surf. A* **2011**, *375*, 23.
[8] K. J. Edgar, *Cellulose* **2007**, *14*, 49.
[9] K. J. Edgar, C. M. Buchanan, J. S. Debenham, P. A. Rundquist, B. D. Seiler, M. C. Shelton, D. Tindall, *Prog. Polym. Sci.* **2001**, *26*, 1605.
[10] F. Fayazpour, B. Lucas, C. Alvarez-Lorenzo, N. N. Sanders, J. Demeester, S. C. De Smedt, *Biomacromolecules* **2006**, *7*, 2856.
[11] T. Radeva, K. Kamburova, I. Petkanchin, *J. Colloid Interface Sci.* **2006**, *298*, 59.
[12] J. Liu, F. He, E. Durham, D. Zhao, C. B. Roberts, *Langmuir* **2008**, *24*, 328.
[13] K. A. Janes, P. Calvo, M. J. Alonso, *Adv. Drug Delivery Rev.* **2001**, *47*, 83.
[14] E. I. Rabea, M. E.-T. Badawy, C. V. Stevens, G. Smagghe, W. Steurbaut, *Biomacromolecules* **2003**, *4*, 1457.
[15] S. Daus, T. Heinze, *Macromol. Biosci.* **2010**, *10*, 211.
[16] S. Hornig, T. Heinze, *Carbohydr. Polym.* **2007**, *68*, 280.
[17] R. J. Hunter, *Zeta potential in colloid science: principles and applications*, Academic Press, London, UK **1981**.
[18] A. V. Delgado, F. González-Caballero, R. J. Hunter, L. K. Koopal, J. Lyklema, *J. Colloid Interface Sci.* **2007**, *309*, 194.
[19] H. Ohshima, *Colloids Surf. A* **1995**, *103*, 249.
[20] J. López-Viota, S. Mandal, A. V. Delgado, J. L. Toca-Herrera, M. Möller, F. Zanuttin, M. Balestrino, S. Krol, *J. Colloid Interface Sci.* **2009**, *332*, 215.
[21] T. Indest, J. Laine, V. Ribitsch, L.-S. Johansson, K. Stana-Kleinschek, S. Strnad, *Biomacromolecules* **2008**, *9*, 2207.
[22] M. Dworkin, *The Prokaryotes: Symbiotic associations, biotechnology, applied microbiology,* Vol. *1*, Springer Science+BusinessMedia Inc., New York **2006**.
[23] S. Mao, X. Shuai, F. Unger, M. Simon, D. Bi, T. Kissel, *Int. J. Pharm.* **2004**, *281*, 45.
[24] B. Lindman, G. Karlström, L. Stigsson, *J. Mol. Liq.* **2010**, *156*, 76.
[25] L. F. Zemljič, D. Čakara, N. Michaelis, T. Heinze, K. S. Kleinschek, *Cellulose* **2011**, *18*, 33.
[26] L. Fras, J. Laine, P. Stenius, K. Stana-Kleinschek, V. Ribitsch, V. Dolesek, *J. Appl. Polym. Sci.* **2004**, *92*, 3186.
[27] A. Nakajima, *J. Lumin.* **1977**, *15*, 277.
[28] I. Banerjee, R. C. Pangule, R. S. Kane, *Adv. Mater.* **2011**, *23*, 690.
[29] H. Fasl, J. Stana, D. Stropnik, S. Strnad, K. Stana-Kleinschek, V. Ribitsch, *Biomacromolecules* **2010**, *11*, 377.
[30] P. Käuper, W.-M. Kulicke, S. Horner, B. Saake, J. Puls, J. Kunze, H.-P. Fink, U. Heinze, T. Heinze, E.-A. Klohr, H. Thielking, W. Koch, *Angew. Makromol. Chem.* **1998**, *260*, 53.